J|A|C|S
ARTICLES

Published on Web 09/22/2010

Crystals in Which Some Metal Atoms are More Equal Than Others: Inequalities From Crystal Packing and Their Spectroscopic/Magnetic Consequences

Michael Nippe,[†] Jingfang Wang,[‡] Eckhard Bill,[§] Håkon Hope,[||] Naresh S. Dalal,*[,‡] and John F. Berry*[,†]

Department of Chemistry, University of Wisconsin - Madison, 1101 University Avenue, Madison, Wisconsin 53706, Department of Chemistry and Biochemistry, Florida State University, P.O. Box 3064390 Tallahassee, Florida 32306, Max Planck Institut für Bioanorganische Chemie, Stiftstrasse 34-36, D-45470 Mülheim an der Ruhr, Germany, and Department of Chemistry, University of California, Davis, One Shields Avenue, Davis, California 95616

Received July 22, 2010; E-mail: berry@chem.wisc.edu; dalal@chem.fsu.edu

Abstract: Crystal structures of the heterometallic compounds $CrCrFe(dpa)_4Cl_2$ (**1**), $CrCrMn(dpa)_4Cl_2$ (**2**), and $MoMoMn(dpa)_4Cl_2$ (**3**) (dpa = 2,2′-dipyridylamide) show disorder in the metal atom positions such that the linear $M_A{\equiv}M_A{\cdots}M_B$ array for a given molecule in the crystal is oriented in one of two opposing directions. Despite the fact that the direct coordination sphere of the metals in the two crystallographically independent orientations is identical, subtle differences in some metal−ligand bond distances are observed in **1** and **3** due to differences in the orientation of a solvent molecule of crystallization. The Fe(II) and Mn(II) ions serve as sensitive local spectroscopic probes that have been interrogated by Mössbauer spectroscopy and high-field EPR spectroscopy, respectively. The subtle differences in the two independent Fe and Mn sites in **1** and **3** unexpectedly give rise to unusually large differences in the measured Fe quadrupole splitting (ΔE_Q) in **1** and Mn zero-field splitting (D) in **3**. Variable-temperature/single-crystal EPR spectroscopy has allowed us to determine that the temperature-dependent **D** tensors in **3** are oriented along the metal−metal axis and that they show significantly different dynamic behavior with temperature. The differences in ΔE_Q and D are reproduced by density functional calculations on truncated models for **1** and **3** that lack the quadruply bonded $M_A{\equiv}M_A$ groups, though the magnitude of the calculated effect is not as large as that observed experimentally. We suggest that the large observed differences in ΔE_Q and D for the individual sites could be due to the influence of the strong diamagnetic anisotropy of the quadruply bonded M≡M unit.

1. Introduction

Heterometallic complexes offer chemical and physical complexity as useful features that are currently of interest to applications in synthesis,[1] catalysis,[2] and molecular magnetism,[3] and are often encountered in natural systems.[4] The nature of interactions (bonded or nonbonded) between two different metals that are held in close proximity is often hard to define, but insights can be gained through systematic variation of the identity of the metals in structurally analogous compounds. In order to gain such insight, we have introduced heterometallic complexes of the type shown in Chart 1 that contain a metal−metal multiply bonded unit in close proximity to a first-row transition metal ion.

It is possible to prepare systematically compounds with Cr≡Cr, Mo≡Mo, W≡W, and Mo≡W multiply bonded groups with appended first-row transition metals Cr^{2+}, Mn^{2+}, Fe^{2+}, and Co^{2+}.[5−7] Structural comparisons of compounds having the same M_A but varying M_B, or vice versa, are useful for gauging the structural influence of heterometallic interactions, for example the *trans* influence.[6] Another feature of the molecules in Chart 1 is that the M_B atoms are paramagnetic, and may therefore serve as spectroscopic probes for electronic structure. Relevant to the results reported here are Fe(II) and Mn(II), which are readily interrogated by Mössbauer and EPR spectroscopy, respectively.

Chart 1

Metal−metal multiply bonded groups are well-known to possess strong magnetic anisotropy.[8] Paramagnetic dimetal complexes with $S > 1/2$ such as Ru_2^{5+} species have unusually large axial zero-field splitting,[9] and quadruply bonded species, such as those in our compounds, have strong diamagnetic

[†] University of Wisconsin - Madison.
[‡] Florida State University.
[§] Max Planck Institut für Bioanorganische Chemie.
[||] University of California, Davis.

anisotropy, which is known to cause well-defined shifts in NMR experiments similar to the ring current in benzene.[10] We are particularly interested in determining if the magnetic anisotropy of the metal−metal bond would have any effect on the anisotropy of the Fe(II) and Mn(II) ions as probed by the Mössbauer quadrupole splitting (ΔE_Q) and zero-field splitting (D), respectively. Thus we present here Mössbauer and EPR studies of the compounds $CrCrFe(dpa)_4Cl_2$ (**1**), $CrCrMn(dpa)_4Cl_2$ (**2**), and $MoMoMn(dpa)_4Cl_2$ (**3**).

The crystal structures of these three compounds are unusual in that they contain more than one crystallographically independent Fe or Mn site. In most cases in which crystals of this type are observed, the molecules may show only slight differences in bond lengths and angles, and in the large majority of these cases the molecules are considered to be chemically equivalent. Indeed, this is the case in compound **2**. In **1** and **3**, however, small geometric differences are observed for the crystallographically independent Fe(II) and Mn(II) ions in the structures. The impact of these structural variations on the spectroscopic features of the molecules is described here including a very detailed assignment of EPR signals from high-field single-crystal EPR measurements. These results could lead to the development of the ability to affect site-specific magnetic excitations and energy transfer in molecular crystals coherently, which are important prerequisites for spin-based quantum computing.

2. Experimental Section

2.1. Materials. All reactions were carried out under a dry N_2 atmosphere using Schlenk techniques and glovebox methods. Solvents diethyl ether (Et_2O), tetrahydrofuran (THF) and hexanes were purified using a Vacuum Atmospheres solvent purification system. Dichloromethane was freshly distilled under an N_2 atmosphere over CaH_2 prior to use. Naphthalene (Sigma-Aldrich) and anhydrous $MnCl_2$ (Strem) were purchased. The $MnCl_2$ was refluxed in THF to yield white $MnCl_2 \cdot 2THF$. The ligand dpaH (2,2′-dipyridylamine, Sigma-Aldrich) was recrystallized from hot hexanes prior to use.

2.2. Synthesis. $Mo_2(dpa)_4$,[6] $Cr_2(dpa)_4$,[5] and $CrCrFe(dpa)_4Cl_2 \cdot CH_2Cl_2$[5] were prepared according to literature procedures.

2.3. $CrCrMn(dpa)_4Cl_2 \cdot CH_2Cl_2$ (2). THF (25 mL) was added to a mixture of solid orange crystalline $Cr_2(dpa)_4$ (200 mg, 0.25 mmol) and white $MnCl_2 \cdot 2THF$ (100 mg, 0.37 mmol). The mixture was stirred and heated to reflux for ∼8 h and subsequently concentrated to ∼10 mL. The microcrystalline brown solid was separated by filtration, washed with hexanes (40 mL) and dried under vacuum. The solid was dissolved in CH_2Cl_2 (25 mL) and the resulting dark brown solution was filtered and layered with hexanes. Crystals grew within 1 day of diffusion. Crystalline yield: 140 mg, 56%. Anal. Calcd. for $C_{40.5}H_{33}Cl_3Cr_2Mn_1N_{12}$ ($CrCrMn(dpa)_4Cl_2 \cdot 0.5CH_2Cl_2$): C, 51.04%; H, 3.49%; N, 17.64%; Mn, 5.76%. Found: C, 51.48%; H, 3.18%; N, 16.91%; Mn, 5.41%. MALDI TOF mass spectrum (100% peak, amu): $m/z = 874$ [M - $Cl^-]^+$, 614 $[Cr_2(dpa)_3]^+$. IR (KBr, cm^{-1}): 2963 vw, 1606 s, 1593 s, 1548 m, 1468 s, 1425 m, 1360 s, 1315 m, 1284 m, 1268 m,1241 w, 1166 m, 1152 s, 1108 w, 1054 w, 1016 m, 974 w, 920 m, 877 m, 859 m, 766 m, 734 m, 635 w, 538 w, 515 w, 441 w, 421 w.

2.4. $MoMoMn(dpa)_4Cl_2 \cdot Et_2O$ (3). Solid red $Mo_2(dpa)_4$ (250 mg, 0.23 mmol) and white $MnCl_2 \cdot 2THF$ (100 mg, 0.37 mmol) were combined with naphthalene (4.00 g) in a Schlenk flask. The flask was placed while stirring into a sand bath that had been preheated to ∼230 °C. The flow rate of the nitrogen inlet stream was reduced to a minimum and the naphthalene that sublimed onto the flask walls was melted using a heat gun. After ∼1 h at 230 °C the color changed to brown and the mixture was cooled to room temperature. The mixture was washed with hot hexanes (2 × 50 mL) to remove the naphthalene and the resulting red-brown solid was dried under vacuum for 30 min. The solid residue was extracted with CH_2Cl_2 (30 mL), and the resulting brown solution was layered with Et_2O. Crystals of **3** were obtained after 1 day. Yield: 80 mg, 32%. Anal. Calcd. for $C_{44}H_{42}Cl_2MnMo_2N_{12}O$ (**2**): C 49.27%, H 3.95%, N

(1) (a) Dikarev, E. V.; Gray, T. G.; Li, B. *Angew. Chem., Int. Ed.* **2005**, *44*, 1721. (b) Dikarev, E. V.; Li, B.; Zhang, H. *J. Am. Chem. Soc.* **2006**, *128*, 2814–2815. (c) Dikarev, E. V.; Zhang, H.; Li, B. *J. Am. Chem. Soc.* **2005**, *127*, 6156. (d) Greenwood, B. P.; Forman, S. I.; Rowe, G. T.; Chen, C.-H.; Foxman, B. M.; Thomas, C. M. *Inorg. Chem.* **2009**, *48*, 6251–6260. (e) Greenwood, B. P.; Rowe, G. T.; Chen, C.-H.; Foxman, B. M.; Thomas, C. M. *J. Am. Chem. Soc.* **2009**, *132*, 44–45. (f) Miller, K. L.; Williams, B. N.; Benitez, D.; Carver, C. T.; Ogilby, K. R.; Tkatchouk, E.; Goddard, W. A., III; Diaconescu, P. L. *J. Am. Chem. Soc.* **2010**, *132*, 342–355. (g) Monreal, M. J.; Diaconescu, P. L. *J. Am. Chem. Soc.* **2010**, *132*, 7676–7683. (h) Zhang, H.; Yang, J.-H.; Shpanchenko, R. V.; Abakumov, A. M.; Hadermann, J.; Clérac, R.; Dikarev, E. V. *Inorg. Chem.* **2009**, *48*, 8480–8488.

(2) (a) Greeley, J.; Mavrikakis, M. *Nat. Mater.* **2004**, *3*, 810–815. (b) Liu, Z.; Jackson, G. S.; Eichhorn, B. W. *Angew. Chem., Int. Ed.* **2010**, *49*, 3173–3176. (c) Rodriguez, J. A.; Goodman, D. W. *Science* **1992**, *257*, 897–903. (d) Wang, J.; Li, H.; Guo, N.; Li, L.; Stern, C. L.; Marks, T. J. *Organometallics* **2004**, *23*, 5112–5114.

(3) (a) Ako, A. M.; Mereacre, V.; Clérac, R.; Hewitt, I. J.; Lan, Y.; Buth, G.; Anson, C. E.; Powell, A. K. *Inorg. Chem.* **2009**, *48*, 6713–6723. (b) Beltran, L. M. C.; Long, J. R. *Acc. Chem. Res.* **2005**, *38*, 325–334. (c) Chandrasekhar, V.; Pandian, B. M.; Vittal, J. J.; Clérac, R. *Inorg. Chem.* **2009**, *48*, 1148–1157. (d) Fishman, R. S.; Okamoto, S.; Miller, J. S. *Phys. Rev. B* **2009**, *80*, 140416(4). (e) Harris, T. D.; Bennet, M. V.; Clérac, R.; Long, J. R. *J. Am. Chem. Soc.* **2010**, *132*, 3980–3988. (f) Harris, T. D.; Long, J. R. *Chem. Commun.* **2007**, 1360–1362. (g) Her, J.-H.; Kennon, B. S.; Shum, W. W.; Stephens, P. W.; Miller, J. S. *Inorg. Chim. Acta* **2008**, *361*, 3462–3464. (h) Kaye, S. S.; Choi, H. J.; Long, J. R. *J. Am. Chem. Soc.* **2008**, *130*, 16921–16925. (i) Liao, Y.; Shum, W. W.; Miller, J. S. *J. Am. Chem. Soc.* **2002**, *124*, 9336–9337. (j) Mereacre, V.; Prodius, D.; Turta, C.; Shova, S.; Filoti, G.; Bartolomé, J.; Clérac, R.; Anson, C. E.; Powell, A. K. *Polyhedron* **2009**, *28*, 3017–3025. (k) Nelson, K. J.; DiPasquale, A. G.; Rheingold, A. L.; Daniels, M. C.; Miller, J. S. *Inorg. Chem.* **2008**, *47*, 7768–7774. (l) Shatruk, M.; Avendano, C.; Dunbar, K. R. *Prog. Inorg. Chem.* **2009**, *56*, 155–334. (m) Shum, W. W.; Her, J.-H.; Stephens, P. W.; Lee, Y.; Miller, J. S. *Adv. Mater.* **2007**, *19*, 2910–2913. (n) Shum, W. W.; Schaller, J. N.; Miller, J. S. *J. Phys. Chem. C* **2008**, *112*, 7936–7938. (o) Tanase, S.; Tuna, F.; Guionneau, P.; Maris, T.; Rombaut, G.; Mathonière, C.; Andruh, M.; Kahn, O.; Sutter, J.-P. *Inorg. Chem.* **2003**, *42*, 1625–1631. (p) Vos, T. E.; Liao, Y.; Shum, W. W.; Her, J.-H.; Stephens, P. W.; Reiff, W. M.; Miller, J. S. *J. Am. Chem. Soc.* **2004**, *126*, 11630–11639. (q) Vos, T. E.; Miller, J. S. *Angew. Chem., Int. Ed.* **2005**, *4*, 2416–2149.

(4) (a) Bollinger, J. M.; Jiang, W.; Green, M. G.; Krebs, C. *Curr. Opin. Struct. Biol.* **2008**, *18*, 650–657. (b) Darensbourg, M. Y.; Lyon, E. J.; Smee, J. J. *Coord. Chem. Rev.* **2000**, *206−207*, 533–561. (c) del Rio, D.; Sarangi, R.; Chufan, E. E.; Karlin, K. D.; Hedman, B.; Hodgson, K. O.; Solomon, E. I. *J. Am. Chem. Soc.* **2005**, *127*, 11969–11978. (d) Ghiladi, R. A.; Chufán, E. E.; del Rio, D.; Solomon, E. I.; Krebs, C.; Huynh, B. H.; Huang, H.-w.; Moenne-Loccoz, P.; Kaderli, S.; Honecker, M.; Zuberbühler, A. D.; Marzilli, L.; Cotter, R. J.; Karlin, K. D. *Inorg. Chem.* **2007**, *46*, 3889–3902. (e) Jiang, W.; Bollinger, J. M.; Krebs, C. *J. Am. Chem. Soc.* **2007**, *129*, 7504–7505. (f) Jiang, W.; Hoffart, L. M.; Krebs, C.; Bollinger, J. M. *Biochemistry* **2007**, *46*, 8709–8716. (g) Jiang, W.; Yun, D.; Saleh, L.; Bollinger, J. M.; Krebs, C. *Biochemistry* **2008**, *47*, 13736–13744. (h) Seefeldt, L. C.; Hoffman, B. M.; Dean, D. R. *Annu. Rev. Biochem.* **2009**, *78*, 701–722. (i) Younker, J. M.; Krest, C. M.; Jiang, W.; Krebs, C.; Bollinger, J. M.; Green, M. G. *J. Am. Chem. Soc.* **2008**, *130*, 15022–15027. (j) Zhang, Y.; Holm, R. H. *J. Am. Chem. Soc.* **2003**, *125*, 3910–3920.

(5) Nippe, M.; Berry, J. F. *J. Am. Chem. Soc.* **2007**, *129*, 12684–12685.

(6) Nippe, M.; Victor, E.; Berry, J. F. *Eur. J. Inorg. Chem.* **2008**, 5569–5572.

(7) Nippe, M.; Victor, E.; Berry, J. F. *Chem. Commun.* **2009**, 4357–4359.

(8) Cotton, F. A. In *Muliple Bonds Between Metal Atoms*, 2nd ed.; Cotton, F. A., Murillo, C. A., Walton, R. A., Eds.; Springer Science and Business Media, Inc: New York, 2005; Vol. 16, p 720.

(9) (a) Chen, W.-Z.; Cotton, F. A.; Dalal, N. S.; Murillo, C. A.; Ramsey, C. M.; Ren, T.; Wang, X. *J. Am. Chem. Soc.* **2005**, *127*, 12691–12696. (b) Telser, J.; Drago, R. S. *Inorg. Chem.* **1984**, *23*, 3114–3120.

(10) (a) Collman, J. P.; Barnes, C. E.; Swepston, P. N.; Ibers, J. A. *J. Am. Chem. Soc.* **1984**, *106*, 3500–3510. (b) Collman, J. P.; Garner, J. M.; Hembre, R. T.; Ha, Y. *J. Am. Chem. Soc.* **1992**, *114*, 1292–1301.

15.67%; found C 49.36%, H 3.37%, N 15.32%. MALDI-Mass spectrum: $m/z = 964$ $[M - Cl]^+$, 874 $[Mo_2(dpa)_4]^+$. IR (KBr, cm^{-1}): 2968 w, 1601 m, 1591 m, 1475 s, 1419 s, 1353 m, 1344 m, 1310 m, 1262 s, 1153 s, 1104 s, 1016 m, 853 w, 803 m, 782 m, 769 m, 751 m, 472 w, 419 w.

2.5. Physical Measurements. Elemental analysis was carried out by Columbia Analytical Services in Tucson, Arizona, USA. The IR spectra were taken on a BRUKER TENSOR 27 using KBr techniques. Mass spectrometry data were recorded at the Mass Spectrometry Facility of the Chemistry Instrument Center of the University of Wisconsin-Madison. Matrix-assisted laser desorption/ionization (MALDI) mass spectra were obtained using a Bruker REFLEX II mass spectrometer equipped with a 337 nm laser, a reflectron, delayed extraction, and a time-of-flight (TOF) analyzer. In the positive ion mode, the acceleration voltage was 25 kV. ^{57}Fe Mössbauer spectra were measured on a conventional spectrometer with alternating acceleration. The γ-radiation source (^{57}Co/Rh, 0.9 GBq) was kept at room temperature. The minimum experimental line widths were 0.24 $mm \cdot s^{-1}$. The temperature of the samples was controlled by an Oxford Instruments Variox Cryostat. Isomer shifts were determined relative to α-iron at 300 K. X-Band EPR spectra of frozen solutions (CH_2Cl_2) of **2** and **3** were recorded at low temperature (~10 K) using a Bruker EleXsys EPR spectrometer: E-500-A console with ER 049SX SuperX Bridge and SuperX Cavity. The sample temperature was set using an Oxford Instruments ESR 900 continuous flow liquid helium cryostat regulated by an Oxford ITC4 temperature controller.

The high-field/high-frequency (HF-EPR) measurements were made using the spectrometers available at the National High Magnetic Field Laboratory in Tallahassee, Florida. Measurements on powder samples were made using a locally constructed spectrometer.[11] Its probe is a transmission-type device based on propagating the millimeter and submillimeter waves in cylindrical light pipes, without any resonant cavity. It covers the frequency range of 95 - 405 GHz. Temperature control is achieved with an Oxford Instruments CF1200 continuous-flow liquid-helium cryostat and an ITC503 controller, over the range of 4−300 K, with a precision of 0.1 K. The detector is a liquid-helium-cooled InSb bolometer from QMC Instruments. Magnetic field modulation is employed with the ensuing phase-sensitive detection using a lock-in amplifier. Single-crystal measurements utilized a multifrequency quasi-optical EPR spectrometer[12] that employs a superheterodyne design with Schottky diode mixer/detectors. It employs a Martin-Pupplett interferometer which can vary the polarization of the millimeter waves incident on the sample from linear to circular polarization. It covers the frequency range of 120−336 GHz. In the cw mode, the highest sensitivity is obtained by applying linearly polarized microwaves and detecting the signal in the cross-polarized reflected mode. Temperature is controlled over the range of 1.27−300 K using also an Oxford Instruments CF-1200 continuous-flow helium cryostat, with a precision of about 0.05 K. The authenticity of the single crystals was checked with an X-ray diffractometer. The crystals were face indexed so that the angles between the magnetic field and molecule chain axes can be tracked as a function of the magnetic field direction. The experimental spectra were compared with those simulated theoretically, using the computer program *SPIN* written by Ozarowski.[13] Simulations are based on the spin Hamiltonian formalism using eq 1.

$$H = g\beta H\hat{S}_z + D\left[\hat{S}_z^2 - \frac{1}{3}\hat{S}^2 + {}^{E}/_{D}(\hat{S}_x^2 - \hat{S}_y^2)\right] \qquad (1)$$

This program involves the diagonalization of the electron Zeeman (g) and the zero-field splitting tensors D and E for a given value of spin in the molecular frame. The spectra are simulated with a given set of g, D and E parameters and a line shape function of a Gaussian or Lorentzian form (or their mixture), and visually compared with the experimental ones, and the parameters are varied until a satisfactory fit is obtained. Spectra at each temperature were simulated this way, yielding spin Hamilton parameters g, D and E. For the case of a powder sample, the simulation process involves constructing a powder pattern, by averaging over all spatial orientations of the single crystal with respect to the magnetic field.[13] The peak intensity was obtained by integrating the area under the peak with the *Origin 8.0* program.

2.6. X-ray Structure Determinations at 97 K. Crystals of **2** and **3** were selected under oil under ambient conditions. Block shaped single crystals were attached to the tip of a nylon loop. The crystals were mounted in a stream of cold nitrogen at ~97 K and centered in the X-ray beam of a Bruker CCD-1000 diffractometer (Mo Kα) using a video camera. The data were successfully indexed by an autoindexing routine built into the SMART program.[14] The structures were solved using direct methods and refined by least-squares refinement on F^2 followed by difference Fourier synthesis. All hydrogen atoms were included in the final structure factor calculation at idealized positions and were allowed to ride on the neighboring atoms with relative isotropic displacement coefficients.

2.7. X-ray Structure Determinations at Liquid He Temperatures. Diffraction data (Mo Kα) were measured on a Bruker diffractometer equipped with an Apex II detector. The low-temperature attachment was a Cryoindustries of America CRYO-COOL-LHE liquid-He based single-stream cooler. Temperatures at the crystal site were measured with a calibrated Si diode before and after data collection. No temperature drift was observed. For **1**, $T = 12.0$ (5) K, and for **2**, $T = 11.0(5)$ K. For **1** the initial structure solution assumed space group *Pnn*2, as for the 97 K data, starting with parameters from that solution. This structure refined to *R*1 just over 8% at convergence. Other indicators of data quality strongly suggested that a better refinement result should be attainable. In addition, numerous violations of space group absences were evident. A solution based on a twinned monoclinic cell with $\beta = 90°$ in space group *Pn* and a disorder model corresponding to the model from the 97 K structure, easily led to satisfactory solution and refinement. For the 12 K structure unequal occupancies for the two orientations were allowed. In the 97 K structure, the CH_2Cl_2 solvent of crystallization is disordered. In the 12 K structure, no sign of disorder is indicated. Inspection of data frames reveals no splitting or broadening of (h0l) reflections, even at the highest diffraction angles. This indicates that within our ability to measure, β does not deviate from 90°. Final R1 = 0.0238.

The data for **2** showed the same systematic absences as seen for **1**. The refined parameters for **1** were therefore used as the starting point for refinement, with Mn in place of Fe. This readily resulted in a satisfactory refinement. In this structure, the CH_2Cl_2 molecule is disordered. Final $R1 = 0.0233$. In both structures bond distances in the core show small differences between the two orientations. Attempts to restrain the geometries in the two orientations to be similar, led to convincingly poorer refinement, and were therefore abandoned.

(11) (a) Cage, B.; Hassan, A.; Pardi, L.; Krzystek, J.; Brunel, L. C.; Dalal, N. S. *J. Magn. Reson.* **1997**, *124*, 495–498. (b) Hassan, A.; Pardi, L.; Krzystek, J.; Sienkiewicz, A.; Goy, P.; Rohrer, M.; Brunel, L. C. *J. Magn. Reson.* **2000**, *142*, 300–312.

(12) (a) Morley, G. W.; Brunel, L. C.; Van Tol, J. *Rev. Sci. Instrum.* **2008**, *79*, 064703(5). (b) Van Tol, J.; Brunel, L. C.; Wylde, R. J. *Rev. Sci. Instrum.* **2005**, *76*, 074101(8) .

(13) (a) Krzystek, J.; Ozarowski, A.; Telser, J. *Coord. Chem. Rev.* **2006**, *250*, 2308–2324. (b) Krzystek, J.; Yeagle, G.; Park, J.-H.; Meisel, M. W.; Britt, R. D.; Brunel, L. C.; Telser, J. *Inorg. Chem.* **2003**, *42*, 4610–4618.

(14) *SADABS V.2.05, SAINT V.6.22, SHELXTL V.6.10 and SMART 5.622*, Bruker-AXS: Madison, WI, 2000−2003.

2.8. Density Functional Theory (DFT) Calculations. Calculations were performed using the ORCA program package.[15] The 97 K crystal structure of **1** was used as a starting point for the truncated model using the Fe atom, its attached chloro ligand, and the four Fe-bound pyridyl rings, which were modified to pyridine ligands by adding H atoms in the appropriate positions. The resulting model, $[Fe(py)_4Cl]^+$ (**1m**), was optimized using the BP86 functional with double-ζ quality basis functions.[16] To calculate Mössbauer parameters, a B3LYP computation with an expanded CP(PPP) Fe basis set was used following the method of Neese.[17] In order to determine the variability of the Mössbauer parameters as a function of the Fe−Cl bond distance, single-point/Mössbauer computations were carried out on **1m** with fixed Fe−Cl bond distances ranging from 2.233 Å to Å 2.383 Å in steps of 0.03 Å. For models of compound **3**, atomic coordinates were taken from sites A and B of the crystal structure (models **3mA** and **3mB**, respectively). Two additional models were constructed that contain the solvent ether molecules (**3mA(Et)** and **3mB(Et)**, respectively). The models contain the Mn atoms, axial Cl, and equatorial pyridine ligands. C−H bond lengths were altered from those refined crystallographically to lengths that are more reasonable computationally (1.10 Å for pyridine C−H bonds and 1.099 Å for ether C−H bonds). Single point and zero-field splitting[18] computations were made using the BP86 functional with TZVP basis sets.

3. Results and Discussion

3.1. Synthesis. Recently, we reported the preparation of heterometallic $CrCrFe(dpa)_4Cl_2 \cdot CH_2Cl_2$ (**1**) from $Cr_2(dpa)_4$ and $FeCl_2$ (dpa =2,2′-dipyridylamide),[5] and it was proposed that the synthesis of other heterometallic trinuclear compounds of the structure $MMM'(dpa)_4Cl_2$ can generally be achieved by metalation of quadruply bonded dinuclear synthons. Indeed, we have utilized this method to synthesize MMCo compounds with M = Cr and Mo[6] and also the group 6 compound $MoWCr(dpa)_4Cl_2$.[7] Here we extend this method further to Mn^{2+} complexes. The reaction of $Cr_2(dpa)_4$ with $MnCl_2 \cdot 2THF$ in refluxing THF furnishes a brown microcrystalline material which was recrystallized from CH_2Cl_2/hexanes mixtures to afford single crystals of $CrCrMn(dpa)_4Cl_2 \cdot CH_2Cl_2$ (**2**) (Scheme 1). Accordingly, the reaction of $Mo_2(dpa)_4$ with $MnCl_2 \cdot 2THF$ in refluxing naphthalene and subsequent workup yields crystals of $MoMoMn(dpa)_4Cl_2 \cdot Et_2O$ (**3**). The high reaction temperature during metalation of $Mo_2(dpa)_4$ is necessary to enable the ligand rearrangement around the Mo≡Mo unit because dimolybdenum complexes with anionic *N*,*N*′-donor ligands are well known to be kinetically inert. Dichromium species are labile, so lower temperatures can be used for the preparation of **1** and **2**. The crystal structure of **1** at 97 K has been previously reported along with magnetic measurements that establish an $S = 2$ ground state for the compound, indicating a high-spin ground state for the ferrous ion.[5] Compounds **2** and **3** were characterized by X-ray crystallography (*vide infra*), MALDI TOF MS and IR spectroscopy and their composition was established by means of elemental analysis.

Scheme 1

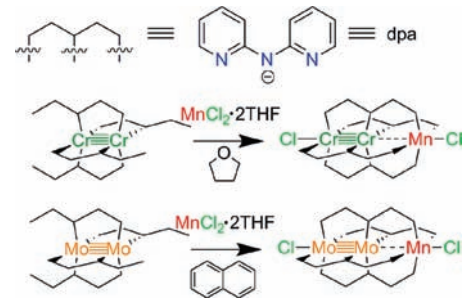

3.2. X-ray Crystallography. All structurally important intramolecular parameters of the Fe in **1** and Mn atoms in **2** and **3** are given in Table 1. Crystallographic details for the structures are given in Table S1 (Supporting Information).

At 97 K, **2** (Figure 1) is isostructural with the earlier described **1** [40] as well as with the homometallic $M_3(dpa)_4Cl_2$ compounds.[19] The molecule crystallizes in the orthorhombic space group *Pnn*2. The metal atoms are disordered over two positions that are related by a crystallographic 2-fold axis, such that both orientations of the molecule are required to be structurally equivalent. The occupancies of the two orientations are therefore also required to be 50% in this space group. The Mn(II) ion displays typical structural features for high-spin Mn(II) ($S = 5/2$), in agreement with the experimentally determined room-temperature magnetic susceptibility of **2** ($\chi \cdot T = 3.90$ emu·K·mol^{-1}). The Mn(II) ion resides in a pseudo octahedral/square pyramidal ligand environment with 4 equatorial pyridine N-atoms (N_{py}) (d(Mn−N_{py}) = 2.190[1] Å), one axial Cl^- ion (d(Mn−Cl) = 2.259(2) Å) and one axial Cr···Mn interaction (d(Mn···Cr) = 2.781(1) Å). The Mn atom is pushed out of the plane of the four pyridine ligands by 0.5 Å, away from the central Cr atom. The Cr−Cr distance of 2.040(1) Å is in good agreement with the distance of 2.025(2) Å observed in **1**, and all other Cr−ligand distances are qualitatively and quantitatively similar to those in **1**. The solvent molecule CH_2Cl_2 in **1** and **2** is disordered over two positions at this temperature.

We had difficulties correlating low-temperature spectroscopic data with the ∼100 K structures of **1** and **2** that feature only one crystallographically independent Fe or Mn site. Therefore, crystallographic investigations of these compounds at lower temperatures were undertaken. When crystallographic analyses of **1** and **2** were performed at 12 and 11 K, respectively, it was found that the systematic absences in the diffraction pattern no longer correspond to *Pnn*2 or any other orthorhombic space group. Instead, the resulting diffraction patterns are best explained by a twinned monoclinic cell with the β angle very close to 90°. The twin law corresponds to a 2-fold rotation along the *a* axis. These observations indicate a phase transition in these crystals, where the symmetry is lowered from orthorhombic to monoclinic as the temperature is lowered. Using this twinned crystal model, the structures were solved and refined in the monoclinic space group *Pn* with no further difficulties. The *Pn* space group lacks the crystallographic 2-fold axis relating one end of the molecules to the other, so in this phase **1** and **2** have two crystallographically distinct Fe and Mn sites, respectively. A similar phase transition is known to occur in the isostructural homometallic tricobalt molecule.[20]

The overall metal−ligand distances of the two orientations in **1** at 12 K and **2** at 11 K vary only marginally from those

(15) Neese, F. *ORCA - An ab Initio, DFT and Semiempirical Electronic Structure Package*, Version 2.6; Universität Bonn: Bonn, 2008.
(16) R. Ahlrichs and co-workers, unpublished work. The Ahlrichs auxiliary basis sets were obtained from the TurboMole basis set library under ftp.chemie.uni-karlsruhe.de/pub/jbasen. Eichkorn, K.; Treutler, O.; Ohm, H.; Haser, M.; Ahlrichs, R. *Chem. Phys. Lett.* **1995**, *240*, 283–289. Eichkorn, K.; Weigend, F.; Treutler, O.; Ahlrichs, R. *Theor. Chem. Acc.* **1997**, *97*, 119–124. Schafer, A.; Horn, H.; Ahlrichs, R. *J. Chem. Phys.* **1992**, *97*, 2571–2577.
(17) Neese, F. *Inorg. Chim. Acta* **2002**, *337*, 181–192.
(18) Ganyushin, D.; Neese, F. *J. Chem. Phys.* **2006**, *125*, 024103(11). Neese, F. *J. Chem. Phys.* **2007**, *127*, 164112(9).
(19) Berry, J. F.; Cotton, F. A.; Lu, T.; Murillo, C. A.; Roberts, B. K.; Wang, X. *J. Am. Chem. Soc.* **2004**, *126*, 7082–7096.

Table 1. Crystallographically Determined Geometric Parameters around the Paramagnetic Transition Metal Ions at 97 K (for **1**, **2**, and **3**) and 12 K for **1** and 11 K for **2**

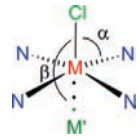

compound	**1**			**2**			**3**	
space group (*T*, K)	*Pnn*2 (97 K)	*Pn* (12 K)		*Pnn*2 (97 K)	*Pn* (11 K)		*P*2(1)/*c* (97 K)	
orientation		1 (47.4(4) %)	2 (52.6(4) %)		1 (47.2(3) %)	2 (52.8(3) %)	1 (69.6(2) %)	2 (30.4(2) %)
M−Cl, Å	2.300(2)	2.347(2)	2.302(2)	2.259(2)	2.251(2)	2.257(2)	2.330(2)	2.321(3)
M−N, Å	2.157[4]	2.151[2]	2.156[2]	2.190[1]	2.197[2]	2.205[1]	2.248[4]	2.256[5]
M···M′, Å	2.715(2)	2.688(3)	2.703(3)	2.781(1)	2.804(3)	2.838(3)	2.790(2)	2.797(5)
M−N_4 plane, Å	0.405	0.367	0.397	0.499	0.511	0.514	0.466	0.456
α, deg	100.82[13]	99.80[7]	100.58[7]	103.1[2]	103.43[7]	103.46[7]	102.0[1]	101.7[2]
β, deg	178.64(15)	178.46(4)	177.97(3)	178.9(4)	178.50(4)	178.41(4)	177.6(1)	178.3(2)

obtained at 97 K (Table 1). The Fe−Cl distances in **1** differ slightly for orientations 1 and 2 by ∼0.05 Å. The Fe−N and Fe···Cr distances, however, are practically identical to within 3*σ* at 2.151[2] and 2.156[2] Å and 2.688(3) and 2.703(3) Å, respectively. The occupancies were refined to be 47.4(4) % and 52.6(4) %. The observation that these are close but not equal to 50/50 suggests a 3% defect of the crystallographic 2-fold axis in **1** at 97 K (similar for **2**, *vide infra*). In contrast to the structure of **1** at 97 K, the solvent CH_2Cl_2 molecule is no longer disordered at 12 K, and the intermolecular Fe···C(CH_2Cl_2) distances are different for the two orientations: 4.97 and 5.13 Å. More importantly, there is a C−H···Cl interaction between the CH_2Cl_2 and the terminal Fe bound Cl^- ion only for orientation 1 and not for orientation 2. The Cl···H(CH_2Cl_2) distance for orientation 1 is 2.75 Å, less than the sum of the van der Waals radii and the C−H···Cl angle is 174°, whereas the shortest Cl···H(CH_2Cl_2) distance is 4.11 Å for orientation 2 with a C−H···Cl angle of 117°. The 0.05 Å elongation of the Fe−Cl bond in orientation 1 as compared to orientation 2 is attributed to this C−H···Cl interaction, which bears similarity to a classical hydrogen bond.

The 11 K structure of **2** reveals structurally almost identical Mn(II) ions for orientations 1 and 2: *d*(Mn−Cl) = 2.251(2) and 2.257(2) Å; *d*(Mn−N) = 2.197[2] and 2.205[1] Å; *d*(Mn···Cr) = 2.804(3) and 2.838(3) Å. The relative occupancies are 47.2(3) % and 52.8(3) % for the two orientations. In contrast to the structure of **1**, the solvent CH_2Cl_2 molecule is, even at this low temperature, disordered and the intermolecular Mn···C(CH_2Cl_2) distances as well as Cl···H(CH_2Cl_2) are similar for both orientations. The orientation of the disordered Cr≡Cr···Mn chains in the unit cell of **2** at 11 K is shown in Figure 2 (top).

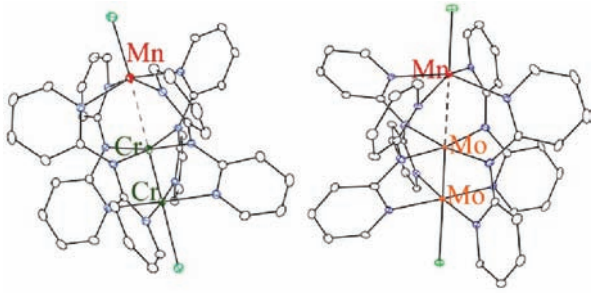

Figure 1. Molecular structures of **2** and **3** with displacement ellipsoids drawn at the 30% probability level. Hydrogen atoms and solvent molecules have been omitted for clarity. Only one molecular orientation is shown.

The crystal structure of **3** was determined at 97 K (Figure 1). The molecule crystallizes in the monoclinic space group $P2_1/c$. The metal atoms are disordered with relative occupancies of oppositely oriented Mo≡Mo···Mn chains of 69.6(2) and 30.4(2). As in the structures of **1** and **2**, there is no sign of disorder in the dpa ligand moieties or the Cl atoms. The two distinct orientations feature small structural differences in the geometry of the metal atoms. The pseudo-octahedral Mn(II) ions in orientations 1 and 2 show very similar Mn−Cl distances of 2.330(4) and 2.321(3) Å as well as Mn−N and Mn···Mo distances of 2.248[4] and 2.256[5] Å and 2.790(2) and 2.797(5) Å, respectively. The presence of a Mo−Mo quadruple bond is established by the Mo−Mo distances of 2.096(2) and 2.104(5) Å. The only major structural difference between the two orientations is the nonbonded intermolecular distance to the solvent molecule: The Mn···O(Et_2O) distances are 6.08 Å and 6.53 Å in orientations 1 and 2, respectively. The orientation of the disordered Mo≡Mo···Mn chains in the unit cell of **3** at 97 K is shown in Figure 2 (bottom). We note that none of the intermolecular H···H distances between the H atoms in 5- and 6-position of the pyridine and the Et_2O H atoms are closer than the sum of their van der Waals radii (2.18 Å).

3.3. Mössbauer Spectroscopy. In order to probe the electronic structure of the Fe(II) nuclei in the high and low temperature

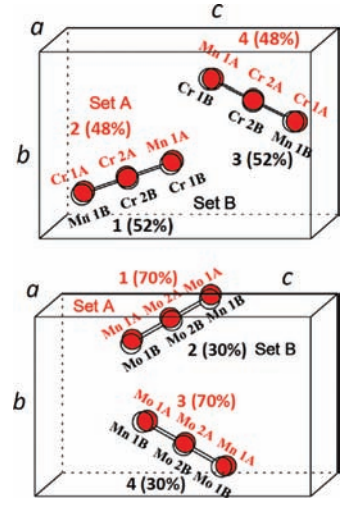

Figure 2. Simplified presentation of the unit cell composition of **2** at 11 K (top) and **3** at 97 K (bottom), showing the metal atom disorder (∼48 and 52 for **2**; ∼70 and 30 for **3**) within the two relative orientations of the trimetallic chains.

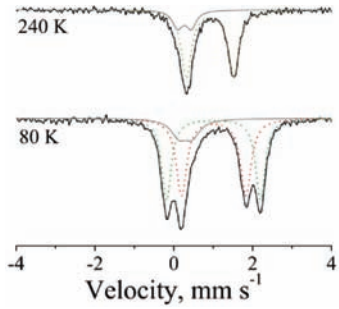

Figure 3. Zero-field Mössbauer spectra of **1** obtained at 240 K (top) and 80 K (bottom). (The gray lines represent an unknown ferric species (14%) with $\delta = 0.3$ mm·s^{-1} and $\Delta E_Q = 0.33$ mm·s^{-1} at 80 K).

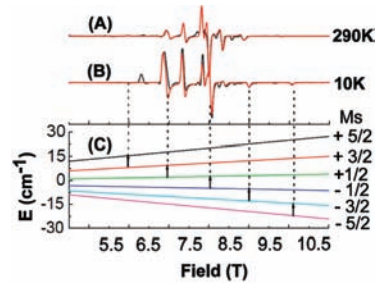

Figure 4. EPR spectra of a KBr pellet of **2** at 216 GHz at 300 and 10 K (A and B) and their peak assignments via simulation (C).

phase of **1**, we recorded Mössbauer spectra at 240 and 80 K (Figure 3). At 240 K a unique quadrupole doublet was detected with a large isomer shift, $\delta = 0.92$ mm·s^{-1}, and moderately large quadrupole splitting, $\Delta E_Q = 1.20$ mm·s^{-1}. The parameters are characteristic of the 3d^6 configuration of high-spin Fe(II) with five or six ligands. (A minor contamination presumably of an unknown ferric degradation product shall be ignored here.) At 80 K, however, two distinct quadrupole doublets are observed, revealing the presence of two independent high-spin ferrous sites with relative intensities of 42 and 58%. A fit with Lorentzian doublets yielded identical isomer shifts, $\delta = 1.01$ mm·s^{-1}, but significantly different quadrupole splitting values, $\Delta E_Q(1) = 2.39$ and $\Delta E_Q(2) = 1.63$ mm·s^{-1}. An alternative fit of two species with equivalent ΔE_Q and different δ is mathematically possible, but leads to physically unreasonable values of δ. The key parameter for the detection of variations in the electronic structure of the Fe ions is the quadrupole splitting. It reflects the asymmetry of electronic charge distribution of Fe and depends critically on the population of the valence orbitals and the distribution of covalent bonds of ligand orbitals interacting with the Fe. In contrast, the isomer shift, which probes the charge density at the iron nucleus, is determined by scalar properties like the population of the valence shell, the number and type of ligands and the average bond distances. Thus, identical isomer shifts as observed above indicate virtually the same overall covalency for the respective Fe sites. The relative intensities of the two Mössbauer subspectra (42/58) are in good agreement with the crystallographic occupancies (47/53) of the two Fe sites determined at 12 K. The slight deviation could be due to minor differences in the Lamb−Mössbauer factors for the two Fe sites. In summary, the two Mössbauer signals strongly corroborate the presence of two crystallographically independent Fe(II) sites at low temperature, according to the crystallographic observation that at 12 K **1** exists in the lower symmetry space group *Pn*. The phase transition from *Pnn*2 must therefore occur in the small temperature range between 80 and 97 K.

The most striking feature of the 80 K Mössbauer spectrum is the actual magnitude of the difference in quadrupole splitting of the Mössbauer subspectra, $\Delta(\Delta E_Q) = 0.76$ mm·s^{-1}, which is unexpected, given the rather modest structural differences between the two independent Fe sites (see Table 1). To put this observation into perspective, a search of the Cambridge Crystallographic Database for six-coordinate iron complexes with $Z' = 2$ (i.e., two independent Fe molecules in the asymmetric unit) was carried out, which yielded more than 50 examples of compounds, for which Mössbauer spectra were recorded. For most cases of ferrous and ferric complexes with qualitatively identical coordination spheres around the two independent Fe atoms, only *one* broad asymmetric feature was observed by Mössbauer spectroscopy, which cannot be unambiguously explained by the inequality of the two Fe sites,[21] but would be consistent with ΔE_Q values for the two sites that are very similar to each other. However, if intermolecular interactions in the form of hydrogen bonding influence the ligand binding to each Fe differently, the two Fe sites then display distinct Mössbauer spectra. Examples of this behavior are found for the high-spin complex (2-methylimidazole)(tetraphenylporphyrinato)Fe(II) ($\delta = 0.92/0.97$ mm·s^{-1}, $\Delta E_Q = 2.40/2.90$ mm·s^{-1})[22] and the high-spin complex Fe(II)L(NCS)$_2$ (L = *N*,*N*′-bis[(1*H*-imidazol-4-yl)methylene]-2,2-dimethylpropane-1,3-diamine) ($\delta = 1.15$ mms^{-1}, $\Delta E_Q = 1.51/2.58$ mm·s^{-1}).[23] The only significant difference for the two Fe sites in **1** stems from the intermolecular C−H···Cl interaction. To our knowledge, this is the first time that such a weak intermolecular interaction has been shown to cause such a significant change in the electronic structure of a metal atom.

3.4. EPR Spectroscopy. Compounds **2** and **3** were investigated by means of variable temperature variable field EPR spectroscopy. The high resolution afforded by high field (240 GHz) EPR spectroscopy revealed very precise details on the magnetic parameters of the individual Mn(II) ions in **2** and **3**. Four issues will be addressed in the following: (1) temperature dependence of powder sample spectra of **2** and **3**; (2) temperature dependence of single-crystal spectra; (3) angular dependence of single-crystal spectra at 2.6 K; (4) temperature dependence of the zero-field splitting parameter *D*.

3.4.1. Temperature Dependence of Powder Samples of 2 and 3. Initial efforts to obtain EPR spectra of **2** and **3** in frozen solution using a conventional X-band frequency (9.5 GHz) yielded spectra with features indicating $D \gg g\beta H$ (Figure S1, Figure S2, Supporting Information), from which only limited information on the spin Hamiltonian parameters could be obtained.

The powder EPR spectra (KBr pellet) of **2** were then obtained at 220.8 GHz in the range between 290 and 10 K (A and B, Figure 4) and the spectra of **3** were collected at 203.2 GHz at temperatures from 260 K down to 10 K (A and B in Figure 5).

(20) Clérac, R.; Cotton, F. A.; Daniels, L. M.; Dunbar, K. R.; Kirschbaum, K.; Murillo, C. A.; Pinkerton, A. A.; Schultz, A. J.; X., W. *J. Am. Chem. Soc.* **2000**, *122*, 6226–6236.

(21) Simaan, A. J.; Boillot, M.-L.; Carrasco, R.; Cano, J.; Girerd, J.-J.; Mattioli, T. A.; Ensling, J.; Spiering, H.; Gütlich, P. *Chem.—Eur. J.* **2005**, *11*, 1779–1793.

(22) Hu, C.; Noll, C. N.; Piccoli, P. M. B.; Schultz, A. J.; Schulz, C. E.; Scheidt, W. R. *J. Am. Chem. Soc.* **2008**, *130*, 3127–3136.

(23) Bréful, N.; Vang, I.; Shova, S.; Dahan, F.; Costes, J.-P.; Tuchagues, J. P. *Polyhedron* **2007**, *26*, 1745–1757.

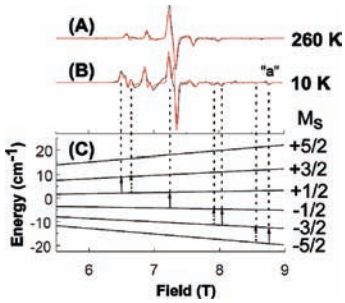

Figure 5. EPR spectra of a KBr pellet of **3** at 203.2 GHz at 260 K (A) and 10 K (B) and their peak assignments via simulation (C). Curves in black are the experimental spectra while those in red are simulations using the parameters listed in the text. The bold and the dashed line arrows indicate the z-transitions of the two sites with the 70:30 statistical populations, respectively (see text and also Figure 7).

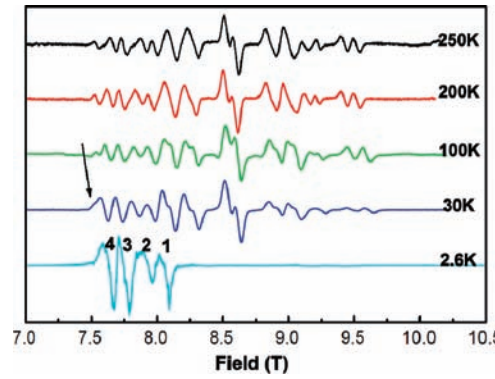

Figure 6. Temperature dependence of single-crystal EPR spectra of **2** with the magnetic field close to the *ab* plane. Note that essentially only four peaks are observed at the lowest temperature, which can be directly assigned to four magnetically distinct Cr≡Cr···Mn molecules, following the numbering scheme of Figure 2.

At this high frequency, many more well-resolved peaks are detected. The best-fit spectra for **2** and **3** are also shown in Figures 4 and 5 (red curves). At 290 K the obtained parameters for **2** ($S = 5/2$) are $g_x = g_y = g_z = 2.000$, $D = 0.449$ cm^{-1}, $E = 0.00747$ cm^{-1}, indicating axial anisotropy of the zero-field splitting, in good agreement with the axial C_4 symmetry of the molecule. The *g*-values obtained for **3** ($S = 5/2$) at 260 K are also very close to the free-electron value ($g_x = g_y = g_z = 2.0023$), but interestingly, two sets of *D* values ($D(1) = 0.324$ cm^{-1}, $D(2) = 0.280$ cm^{-1}) are observed with the same $E = 0.00747$ cm^{-1}, indicating the presence of at least two magnetically distinct Mo≡Mo···Mn molecules in the sample, with axial zero-field splitting. The powder EPR spectra of both **2** and **3** display strong temperature dependence. Peak assignments were made by computer simulation,[13] yielding the energy level diagrams shown in Figures 4 and 5.

The parameters for **2** at 10 K are $g_x = 1.993$, $g_y = 1.991$, $g_z = 1.990$, $D = 0.498$ cm^{-1}, $E = 0.00747$ cm^{-1}. It is noteworthy that the ground-state transition shifts from 9.814 T at 290 K to 10.069 T at 10 K due to an increase in the *D* value. The peaks labeled as "*" are assigned to minor impurities of an air-oxidized component, as their intensities vary from pellet to pellet and over time. We note that only one set of *D* values is observed, indicating that all Mn(II) ions are chemically equivalent at the resolution of these powder measurements. It is noteworthy that at 290 K, all five *z*-oriented $\Delta M_s = 1$ transitions (arrows in Figure 4) are observed, indicating significant Boltzmann population of the higher energy levels at high temperatures. At 10 K the peak at the lowest field side becomes undetectable and the peak at the highest field increases, indicating that the former originates from transitions between the highest energy levels and the latter from the ground state. This assignment in turn establishes that *D* is positive, which is usually the case for six-coordinate mononuclear Mn(II) complexes such as the octahedral *trans*-dichloro complex Mn(γ-picoline)$_4$Cl$_2$[24a] ($D = +0.186$ cm^{-1}) and the monochloro compound [MnClL][PF$_6$] (L = *N*-methyl-*N*,*N*′,*N*′-tris(2-pyridylmethyl)propane-1,3-diamine) ($D = +0.157$ cm^{-1}).[24b] The magnitude of *D* in **2** is with 0.498 cm^{-1} significantly higher than those observed for the former six-coordinate Mn(II) compounds and even higher than the reported *D* value of $+0.25$ cm^{-1} for the distorted square-pyramidal [MnCl(tmc)][BPh$_4$] (tmc = tetramethylcyclam).[24c] The central three transitions in **2** overlap with the signals from the x and y directions.

Lowering the temperature to 10 K also changes the EPR parameters of **3**: $g_x = g_y = g_z = 1.993$, $D_1 = 0.352$ cm^{-1}, $D_2 = 0.294$ cm^{-1} and $E = 0.00747$ cm^{-1}. In contrast to the case of **2**, two nonequivalent Mn(II) sites are clearly present here, with significantly different *D* values. Simulations of the 10 K spectra of **3** (Figure S3, Supporting Information), which include the observed peak intensity ratio of 70% (i in Figure S3, Supporting Information) and 30% (ii in Figure S3, Supporting Information) for orientations 1 ($D_1 = 0.352$ cm^{-1}) and 2 ($D_2 = 0.294$ cm^{-1}) match the experimental data reasonably well. The spectroscopically determined intensity ratio of 70/30 is exactly the same as the crystallographically observed occupancies for the two orientations. The intensity of the ground state transition increases at low temperature, indicating a positive *D* value and shifts to 8.768 T (from 8.5688 T at 260 K), due to an increase in the *D* value at low temperature.

Thus, the powder results for **2** and **3** suggest the presence of one and two magnetically distinct Mn(II) sites for **2** and **3**, respectively, and indicate temperature dependence of the *D* values for both compounds. Crystal structures of both **2** and **3** contain two independent Mn(II) sites, which are shown to be magnetically equivalent for **2**, but, interestingly, inequivalent for **3**. Additionally, much more precise information on the assignment of the *D* values to the independent sites in **2** and **3** was obtained from single-crystal measurements (*vide infra*).

3.4.2. Temperature Dependence of Single-Crystal Spectra of 2 and 3. The temperature dependence of the single-crystal spectra of **2** and **3** are shown in Figures 6 and 7. At higher temperatures (>250 K), there are more than 10 peaks, making the assignment of the spectra difficult. At 2.6 K only 4 dominant signals are obtained for **2** and **3**. These originate from $M_s = -5/2 \rightarrow -3/2$ ground-state transitions of the four magnetically distinct molecular orientations. Integration of the 4 peaks obtained for **2** yields a peak intensity ratio of 49/51 for peaks 1 and 2 (from set A in Figure 2) or 3 and 4 (set B), which is in very good agreement with the relative occupancies of 47% and 53% observed by crystallography. The 69.6(2)/30.4(2) disorder of the Mo≡Mo···Mn chain in the crystal structure of **3** is also quantitatively reproduced by the relative peak intensities

(24) (a) Lynch, W. B.; Boorse, R. S.; Freed, J. H. *J. Am. Chem. Soc.* **1993**, *115*, 10909–10915. Wood, R. M.; Stucker, D. M.; Jones, L. M.; Lynch, W. B.; Misra, S. K.; Freed, J. H. *Inorg. Chem.* **1999**, *38*, 5384–5388. (b) Hureau, C.; Groni, S.; Guillot, R.; Blondin, G.; Duboc, C.; Anxolabéhère-Mallart, E. *Inorg. Chem.* **2008**, *47*, 9238–9247. (c) Bucher, C.; Duval, E.; Barbe, J.-M.; Verpeaux, J.-N.; Amatore, C.; Guilard, R.; Le Pape, L.; Latour, J.-M.; Dahaoui, S.; Lecomte, C. *Inorg. Chem.* **2001**, *40*, 5722–5726.

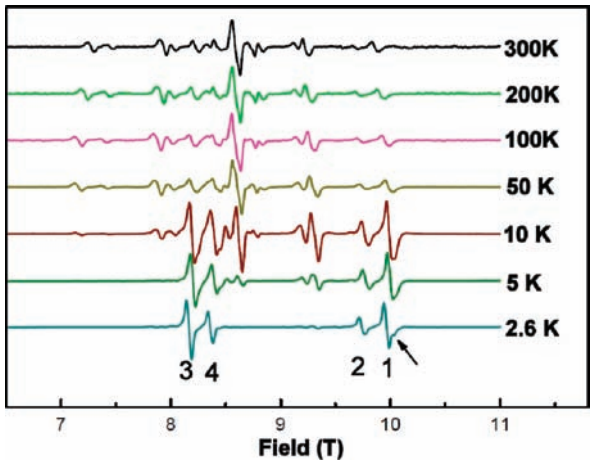

Figure 7. Temperature dependence of single-crystal EPR spectra of **3** with the magnetic field in the (−1, −1, 1) plane. Note that essentially only four peaks are observed at the lowest temperature, which can be directly assigned to four magnetically distinct Mo≡Mo···Mn, following the numbering scheme of Figure 2. The arrow highlights the shoulder that is tentatively ascribed to a phase transition below 10 K.

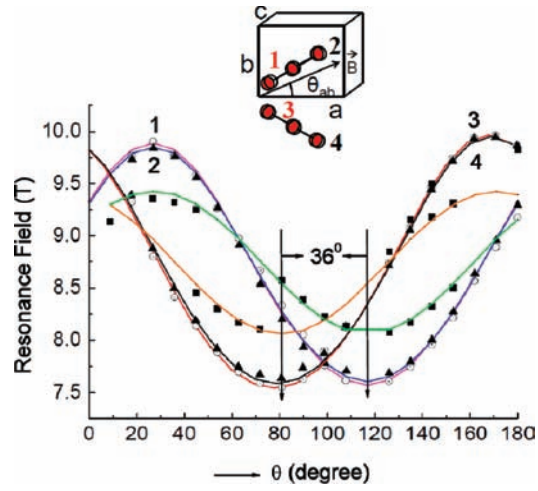

Figure 8. Angular dependence of EPR peaks from **2** at 2.6 K with the field orientated close to the *ab* plane. The pink and blue curves are assigned to molecules 1 and 2 (set A), and the red and black curves are from the molecules 3 and 4 (set B). Green and brown lines are due to the first excited-state transition $M_s = -3/2 \rightarrow M_s = -1/2$.

observed for **3** at 2.6 K: the ratio of peak 1 to peak 2 is 71/29 and the ratio of peak 3 to peak 4 is 67/33. Low-intensity features are present in the spectra of both compounds at 2.6 K, corresponding to transitions between higher energy, sparsely occupied magnetic states ($M_s = -3/2 \rightarrow M_s = -1/2$). As expected, these peaks are of much lower intensity, compared to the other four ground state transitions, following the Boltzmann distribution. For **2** the peaks broadened below 100 K, which is indicative of the crystallographically established phase transition (see above). For **3**, a small shoulder on peak 1 in Figure 7 can be seen (highlighted by an arrow), which may also indicate a phase transition below 10 K, though crystallographic support for this assignment is lacking.

3.4.3. Angular Dependence of Single-Crystal Spectra of 2 and 3 at 2.6 K. To assign the four peaks to the four magnetically distinct molecular orientations in the unit cell of **2** and **3** and to gain information about the directions of the *D* tensors, EPR spectra were measured of the single crystals at 2.6 K with the crystal symmetry axes oriented at several known angles relative to the magnetic field. In the angular dependent spectra of **2**, there are two peaks close to each other at all angles. They follow curves 1 and 2 (Figure 8) with the same angular variation trend with their maximum resonance field obtained at an angle of 29°. Additionally, there are two neighboring peaks following curves 3 and 4, sharing a similar rotational pattern, reaching maximum resonance fields at 171°. Although similar maximum and minimum resonance fields are obtained for these four signals, the angular dependence patterns for curves 1 and 2 are different from those of 3 and 4. It is thus clear that curves 1 and 2 arise from one orientation of disordered Cr≡Cr···Mn molecules (set A and B in Figure 2) while 3 and 4 are from the other orientation. This deduction is rationalized by the above-mentioned peak intensity ratio between 1 and 2 (or 3 and 4) of about 49: 51 at all angles. The only marginally different maximum and minimum resonance fields for sets A and B indicate that their *D* values are nearly the same, in good agreement with the almost identical orientations of the two disordered Cr≡Cr···Mn chains (178.66° and 178.50° for set A and B, respectively). By simulating the experimental angular dependence data, two slightly different *D* values of 0.504 cm^{-1} (set A) and 0.486 cm^{-1} (set B) were found with the same

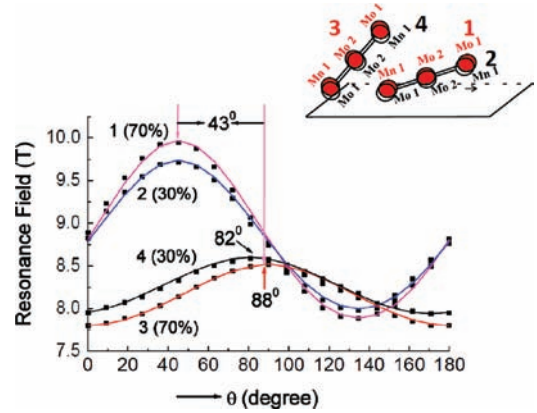

Figure 9. Angular dependence of the HF-EPR peaks from **3** at 2.6 K with the field oriented close to the (−1, −1, 1) plane. The pink and blue curves are assigned to molecules 1 and 2 (set A), the red and black curves are from molecules 3 and 4 (set B).

g-tensors, *E*-values and angles between the magnetic field and the molecular chain axes. The continuous curves in Figure 8 are those calculated theoretically from the spin Hamiltonian parameters (*g*-tensor, *D* and *E* values) obtained from the above simulation at 2.6 K, which match the experimental data exceptionally well. Thus the pink, blue, red, and black curves correspond to molecular orientations 1, 2, 3, and 4, respectively. Additionally, there are two curves in green and brown, which involve $M_s = -3/2 \rightarrow M_s = -1/2$ transitions from set A and set B molecules (see above).

The single-crystal spectra of **3** at various angles show also two different pairs of signals from sets A and B, which are in close proximity to each other at all angles (Figure 9). The angular dependence patterns for peaks 1 and 2 are very different from those of peaks 3 and 4, and in stark contrast to the results obtained for compound **2**, the signal pairs show strongly different maximum and minimum resonance fields. It is thus clear that curves 1 and 2 are from one orientation (A or B) while 3 and 4 are from the other orientation. This deduction is again rationalized by the peak intensity ratio of 71/29 (curve 1/2) and 67/33 (curve 3/4) which is in agreement with the crystallographic data. Utilizing the same approach as for **2**, we

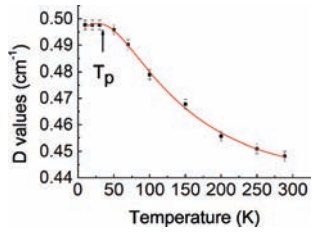

Figure 10. Temperature dependence of the average D values of all the four molecules in **2** (■) with an error bar of 0.001 cm^{-1} for the 4 molecules and their fit to eq 1 (red line). See text for parameters. The arrow highlights the temperature of onset of a structural phase transition.

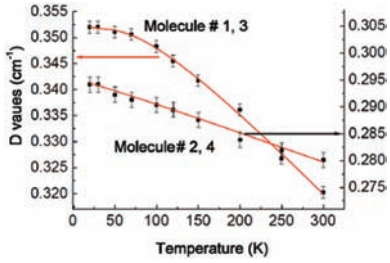

Figure 11. Temperature dependence of D in **3** for the molecules 1 and 3 (set A), and its fit to eq 1 (red curve), with the parameters listed in the text. D values for molecules 2 and 4 (set B) show a quite different temperature dependence (see text).

obtain now a D value of 0.353 cm^{-1} for set A molecules 1 and 3 and 0.294 cm^{-1} for set B molecules 2 and 4, respectively. The calculated curves in Figure 9 are pink and blue for set A while the red and the black curves are from set B. The large difference in D values (0.059 cm^{-1}) for the two orientations is remarkable and manifests the magnetic inequality of the two independent Mn(II) ions.

For HF-EPR spectra at each orienation, the angles between the magnetic field and the principal direction of the **D** tensor from simulation match the actual angles between the magnetic field and the metal chain axis from the crystal structure. Thus the main axis of the **D** tensor is directed along the trimetallic chain for each molecule. In all, a close examination of the angular dependence of EPR peaks enables us to determine the directions and magnitudes of the **D** tensors for each molecule individually. We note that the high resolution provided by employing high frequency EPR spectroscopy complements and expands upon the insights gained from variable temperature X-ray diffraction and Mössbauer spectroscopy experiments.

3.4.4. Temperature Dependence of *D* in 2 and 3. The experimental spectra exhibit strong temperature dependence of the magnetic parameters, in particular the zero-field splitting (D). Measurements were carried out on powdered pellet samples at several temperatures between 10 and 290 K for **2** and 4 and 298 K for **3**. These spectra were simulated and D and E values were obtained combining the single-crystal data. Figure 10 shows the temperature dependence of average D values of the disordered molecules in **2**. The average value is taken here because the difference of the D values from the two sets is too small (0.018 cm^{-1} at 2.6 K) to be accurately assigned to the two sets above 10 K. Figure 11 shows the temperature dependence of the D values for set A (molecules 1,3) and set B (molecules 2,4) in **3**. On lowering the temperature, the D value changes rapidly at first. For **2** it levels off at around 30 K and for **3** at ~50 K.

Such a variation of the D value has been observed before for Mn^{2+} in $CdCl_2$ crystals[25] and a phenomenological model was proposed,[26] which may be used to interpret our data here. In this model, the temperature dependence of the zero-field splitting results from at least two parts. The first static part (D_1) is related to the thermal expansion of the lattice, accounting for uniform changes in bond lengths and bond angles. The second part (D_2) is due to vibrational effects or the structural influence of electron−phonon interactions including acoustic phonons and optical phonons. Using the simplified static and vibrational models,[27] one can write:

$$D = D_0 + D_1 \cdot T + D_2 \exp(-\Delta U/T) \qquad (2)$$

The first two terms come from the static part, in which D_1 is associated with the lattice expansion coefficient, while the last term originates from vibrational contributions. D_2 is an adjustable parameter which describes the strength of the electron−phonon interaction, and ΔU represents the effective barrier, considering only a two-level system. The fit for compound **2** according to eq 2 (red curve in Figure 10), yields the following best-fit parameters: $D_0 = 0.496 \pm 0.001$ cm^{-1}, $D_1 = -0.8 \pm 0.2$ G K^{-1}, $D_2 = -0.124 \pm 0.002$ cm^{-1}, $\Delta U = 165 \pm 5$ K. The important parameter obtained from Figure 10 is the value of the energy barrier ΔU, which is a general measure of phonon energies affecting the zero-field splitting. The small magnitude of the phonon frequency (165 K, or 120 cm^{-1}) implies that this must come from the heavy ions, i.e. vibrations of the Cr≡Cr···Mn chain itself. The same D_0, D_1, D_2, and ΔU values can be used to model signals 1−4 for compound **2**, consistent with the nearly identical environment of the Mn ions in the disordered Cr≡Cr···Mn chains.

We used the same procedure to fit the experimental D values in compound **3**. The best-fit parameters for the two set A molecules 1 and 3 (70% abundance) are $D_{0a} = 0.355 \pm 0.001$ cm^{-1}, $D_{1a} = -1.8 \pm 0.1$ K^{-1}, $D_{2a} = 0.020 \pm 0.002$ cm^{-1}, $\Delta U_a = 70 \pm 8$ K. For the two set B molecules 2 and 4 we obtain: $D_{0b} = 0.295 \pm 0.001$ cm^{-1}, $D_{1b} = -0.415 \pm 0.2$ K^{-1}, $D_{2b} = -0.007 \pm 0.010$ cm^{-1}, $\Delta U_b = 210 \pm 70$ K. The accuracy of the parameters employed in the model for molecules 2 and 4 is much lower than for molecules 1 and 3, due to the minimal change in D of only 0.014 cm^{-1} over the experimental temperature range. Nevertheless, given the structural similarity of the Mn(II) ions in orientations 2 and 4 vs 1 and 3, it is surprising that the two oppositely aligned Mo≡Mo···Mn chains exhibit significantly different motional dynamics and zero-field splitting parameters.

3.5. Density Functional Theory Calculations. The experimental results presented above indicate unusual sensitivity of the spectroscopic parameters (quadrupole splitting and zero-field splitting) to what one would normally consider to be very minor structural differences in **1** and **3**. Compound **2** exhibits more "normal" behavior, with nearly identical structural and magnetic features, whereas weak intermolecular interactions in **1** and **3** result in slight structural differences that have surprisingly large spectroscopic consequences. Quadrupole splitting and zero-field splitting both have their origin in molecular anisotropy. The former effect arises from

(25) Zheng, W. *J. Phys C: Solid State Phys* **1987**, *20*, L697–L701.
(26) Zheng, W.; Wu, S. *J. Phys: Condens. Matter* **1997**, *9*, 5081–5088.
(27) del Barco, E.; Kent, A. D.; Hill, S.; North, J. M.; Dalal, N. S.; Rumberger, E. M.; Hendrickson, D. N.; Chakov, N. E.; Christou, G. *J. Low Temp. Phys.* **2005**, *140*, 119–174.

Chart 2

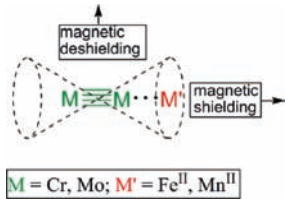

Chart 3

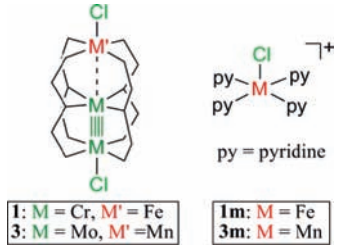

asymmetry in the electric field gradient (EFG) at the Fe nucleus, and zero-field splitting arises from geometric anisotropy of a molecule. The similarity between these two effects is apparent from the spin Hamiltonian terms from which they are derived (eqs 3 and 4).

$$\hat{H}_{\mathrm{Q}} = \frac{eQV_{zz}}{4I(2I-1)}\left[3\hat{I}_z^2 - \hat{I}^2 + \frac{\eta}{2}(\hat{I}_+^2 + \hat{I}_-^2)\right] \qquad (3)$$

$$\hat{H}_{\mathrm{ZFS}} = D\left[\hat{S}_z^2 - \frac{1}{3}\hat{S}^2 + {}^{E}/_{D}(\hat{S}_x^2 - \hat{S}_y^2)\right] \qquad (4)$$

In the above equations, I and S are nuclear and electronic spin functions, respectively. The parameters eQ and V_{ZZ} are the electric quadrupole moment and the principal component of the electric field gradient tensor, respectively, with η being the asymmetry parameter of the EFG tensor. When $\eta = 0$, the quadrupole splitting is defined as $\Delta E_{\mathrm{Q}} = eQ \cdot V_{ZZ}/2$.

It is well-known from NMR studies that metal−metal quadruple bonds have a strong magnetic anisotropy (Chart 2).[8,10] The Fe(II) and Mn(II) ions in **1** and **3** both lie in a region of space that is strongly affected by the magnetic anisotropy of the M≡M quadruple bond. We thus surmise that the quadrupole and zero-field effects of Fe(II) and Mn(II) may be influenced by the presence of the M≡M bond, thereby amplifying small changes that would otherwise not be observable. A preliminary test of the above hypothesis involves using density functional theory (DFT) to calculate the spectroscopically observable features (ΔE_{Q}, and D) for models of **1** and **3** that do not contain M≡M bonded groups. The truncated models **1m** and **3m** involved are shown in Chart 3. Ideally, calculated results of ΔE_{Q} and D for **1m** and **3m** can be compared to those parameters calculated for the whole molecules. At this time, however, the heterotrimetallic molecules are, lamentably, computationally intractable. Successful modeling of their electronic structure most likely necessitates a multideterminantal approach that is currently prohibitively expensive. Thus, we will discuss here only the results of computational work on the monocationic tetrapyridine model compounds **1m** and **3m**.

The optimized Fe−Cl bond length of 2.233 Å in **1m** is significantly shorter than the observed distances, and the Fe−N distance of 2.187 Å is slightly longer. The latter observation is in accord with the well-known propensity of DFT to overestimate metal−nitrogen−ligand bond lengths. The former observation, however, is likely the result of two main factors: (1) As we have previously observed for M≡M···Co compounds, the M≡M axial "ligand" exerts a *trans* influence on the axial chloro ligand.[6] Thus, the calculated **1m**, which is devoid of this interaction, displays a more normal Fe−Cl distance. (2) A second contracting factor for the Fe−Cl bond is the fact that **1m** represents a cationic species, though **1** is a neutral molecule. Greater electrostatic attraction of the negatively charged Cl^- ligand to the positively charged Fe^{2+} ion likely contributes to the shortness of the calculated Fe−Cl bond length.

Table 2. Calculated δ and ΔE_Q for **1m** at Various Fe−Cl Distances

Fe−Cl, Å	δ, mm s^{-1}	ΔE_{Q}, mm s^{-1}	total energy, eV
2.233	0.85	3.97	−73923.90077
2.263	0.86	4.06	−73923.90826
2.293	0.86	4.15	−73923.90559
2.323	0.87	4.24	−73923.89460
2.353	0.88	4.32	−73923.87657
2.383	0.88	4.40	−73923.85236

Consistent with the major structural differences between **1** and **1m**, there are significant differences between the calculated and experimentally observed Mössbauer parameters. The calculated isomer shift of 0.85 mm·s^{-1} is significantly lower than the experimentally observed value of 1.01 mm·s^{-1}, implying that the Fe center in **1** is more electron rich than the Fe center in the model **1m**. This interpretation is corroborated by electrochemical data for **1**, which show that the $Fe^{2+/3+}$ redox couple lies at a more accessible potential in **1** than for other structurally related compounds that lack the Cr≡Cr "ligand".[5] The calculated ΔE_Q of 3.97 mm·s^{-1} is much larger than either value observed for **1** at 80 K, consistent with the lower effective coordination number of **1m** with respect to **1**. As discussed above, the major structural difference between the two independent Fe atoms in the low-temperature structure of **1** is the Fe−Cl bond distance (2.347(2) Å; 2.302(2) Å), which is elongated at one site due to a C−H···Cl interaction with CH_2Cl_2. Therefore, we have used the model **1m** to test the influence of elongating the Fe−Cl bond on the Mössbauer parameters δ and ΔE_{Q} (Table 2). This experiment was carried out by systematically increasing the Fe−Cl bond length in **1m** iteratively by 0.03 Å to a final value if 2.383 Å, calculating values of δ and ΔE_Q for each step. In changing the Fe−Cl distance in **1m** from 2.293 Å to 2.353 Å we observe essentially no consequential change of δ, in agreement with identical δ values observed experimentally for the two species in **1**, but an increase of ΔE_{Q} by 0.17 mm·s^{-1}. This small change of ΔE_{Q} is about half the value of the spectral line width Γ, and would therefore be unresolved under our experimental conditions, in

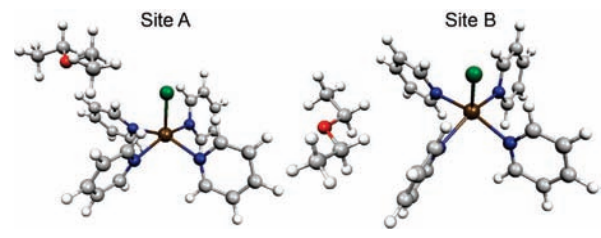

Figure 12. Truncated models of **3** for site A (**3mA(Et)**, left) and B (**3mB(Et)**, right) employed in DFT calculations.

Table 3. Calculated **g** and **D** Tensors for $[(Pyridine)_4MnCl]^+$ Models for Sites **A** and **B** of Compound **3**, along with Experimentally Observed Values

	3mA	3mB	3mA(Et)	3mB(Et)	3A (exp.)	3B (exp.)
Mn−Cl, Å	2.33	2.32	2.33	2.32	2.33	2.32
Mn−N, Å	2.24 − 2.27	2.21 − 2.30	2.24 − 2.27	2.21 − 2.30	2.24 − 2.27	2.21 − 2.30
Mn−(N_4-plane), Å	0.47	0.46	0.47	0.46	0.47	0.46
Mn···O, Å	−	−	6.08	6.53	6.08	6.53
N−Mn−N, deg	82 − 91	85 − 90	82 − 91	85 − 90	82 − 91	85 − 90
N−Mn−Cl, deg	99 − 104	100 − 104	99 − 104	100 − 104	99 − 104	100 − 104
ΔE, rel, kJ/mol	0	+ 5	0	+ 19	−	−
g	2.003	2.003	2.003	2.003	1.993	1.993
D, cm^{-1}	0.866	0.725	0.743	0.725	0.355	0.294
E/*D*	0.008	0.006	0.008	0.006	0.02	0.02

good agreement with what happens in most other compounds. The experimentally determined difference of ΔE_Q for the two Fe sites in **1**, 0.76 $mm \cdot s^{-1}$, is more than 3 times larger. These results imply two conclusions: (1) we can assign the higher ΔE_Q species in the Mössbauer spectrum of **1** to the orientation with the longer Fe−Cl distance; (2) the extent to which ΔE_Q changes upon axial elongation of the Fe coordination sphere may indeed be magnified by the presence of the M≡M unit, though the extent to which this takes place is unclear.

In an effort to elucidate the electronic origin of the unexpected variance of *D* values for the two nonequivalent Mn(II) ions in **3**, truncated computational models, **3m**, for the two distinct Mn sites in **3** were constructed using coordinates from the 11 K crystal structure. Calculations were performed with the crystallographically determined geometries of sites A and B in **3**. To test the effect of the solvent molecule on the ZFS, **3m** was calculated both with (**3mA(Et)** and **3mB(Et)**, Figure 12) and without (**3mA** and **3mB**) the ether molecules present.

The positions of all atoms in the calculations were fixed and the geometry was not optimized. Site **A** has the shorter intermolecular Mn···O distance to the ether molecule, 6.08 Å, and site **B** has the longer distance, 6.53 Å. For the **3m** models, site **A** is calculated to be lower in energy than site **B** by ∼5 kJ/mol (Table 3). The energy difference is enlarged to ∼19 kJ/mol when the ether molecule is included. Though these results do not include vibrational and zero-point energy corrections, they are consistent with the experimental **A**:**B** ratio of 70:30 observed in the crystal structure of **3** and the peak intensity ratio determined by EPR spectroscopy. The calculated (isotropic) *g* values are consistent with those seen experimentally and agree with the interpretation that there is little deviation from the free electron value. Calculated *D* values are larger than those seen experimentally by roughly a factor of 2, which is larger than typical computational errors observed for Mn(II) complexes.[28] We attribute this error to the truncation of **3** to the model compounds **3m**.

The crystallographic results show that there are only minute differences in the coordination geometry of the Mn ions in sites **A** and **B**, yet there is a large difference, $\Delta D \approx 0.0607$ cm^{-1}, in the *D* values measured for the two sites by high-field EPR. *D* values for **3mA** and **3mB** were computed to test whether or not the small geometric differences in the crystal structure can lead to a difference in *D* of this order of magnitude. Indeed, ΔD for **3mA** and **3mB** is ∼0.0299 cm^{-1}, which is somewhat smaller than that observed experimentally, though site **A** is correctly predicted to have the larger *D* value. Addition of ether molecules in crystallographically established distances (i.e., Mn·····O separations of 6.08 and 6.53 Å for sites **A** and **B**, respectively) did not change the *D* value for site **B** (D(**3mB**) = D(**3mB(Et)**)= 0.725 cm^{-1}), as we expected. However, addition of the ether molecule to site A surprisingly lowers the calculated *D* value by 130 G (D(**3mA**) = 0.755 cm^{-1}, D(**3mA(Et)** = 0.743 cm^{-1}). The effect of the ether molecule (with no contact to the **3mA** model shorter than the sum of the van der Waals radii of neighboring atoms) on *D* in site **A** is also evidenced by the calculated Mulliken spin population on the ether oxygen atom. For **3mB(Et)**, a very small spin population of 8.7×10^{-5} appears in the O p orbitals, but for **3mA(Et)** the spin population is about twice as large, 16×10^{-5}. Remarkably, these results show that a seemingly innocent and nonbonded solvate molecule can exert an influence on the magnetic properties and molecular dynamics of a magnetic molecule. Such effects have been noted in the case of magnetic clusters with very high spin, such as Mn_{12}-acetate.[27,29,30] In this case, two CH_3COOH solvent molecules are in close proximity to a Mn_{12}-acetate unit. Without the two acetic acid molecules, Mn_{12} has S_4 point symmetry. With the solvates included, Mn_{12}-acetate was found to have four different geometries by X-ray diffraction.[29] These four structures were predicted to have four different *D* and *E* values, with the maximum difference of 0.028 cm^{-1} and 0.003 cm^{-1} for *D* and for *E*, respectively. Such differences in *D* and *E* values were supported by HF-EPR spectroscopy.[30] We note that the solvent effect of *D* values in Mn_{12}-acetate is smaller than that found in complex **3**, despite the fact that the CH_3COOH molecules engage in strong hydrogen bonds to the Mn_{12}-acetate cluster.[29]

For both the Fe and Mn complexes, DFT calculations of ΔE_Q and *D* of the truncated models reproduce the trends seen experimentally, but the magnitude of the effects are calculated to be different from those observed experimentally. These results suggest that the small effects that slightly alter ΔE_Q and *D* may be magnified by the M≡M multiply bonded unit, though this hypothesis remains to be rigorously tested. A further, quantitative physical model is needed to rationalize these observations.

4. Summary and Concluding Remarks

Variable-temperature X-ray diffraction experiments conducted on single crystals of **1** and **2** evidence a phase transition from the orthorhombic space group *Pnn*2 to monoclinic *Pn* at low temperatures. Lowering the symmetry generates two independent orientations of the Cr≡Cr···Fe and Cr≡Cr···Mn chains in **1** and **2**, respectively. The slightly different geometries of sites A and B result in two signals in the Mössbauer spectrum of **1** with identical δ and surprisingly large differences of ΔE_Q.

(28) Zein, S.; Duboc, C.; Lubitz, W.; Neese, F. *Inorg. Chem.* **2008**, *47*, 134–142.

(29) Cornia, A.; Sessoli, R.; Soraci, L.; Gatteschi, D.; Barra, A.-L.; Daiuebonne, C. *Phys. Rev. Lett.* **2002**, *89*, 257201–257204.

However, HF-EPR experiments reveal very similar D values for the two independent orientations within **2**. In contrast to compound **2**, the two crystallographically independent orientations of Mo≡Mo···Mn chains in **3** contain magnetically different Mn(II) ions (D(A) = 0.353 cm^{-1}, D(B) = 0.294 cm^{-1}), even though the coordination geometries around the two Mn atoms are essentially the same. Furthermore, both sites exhibit different dynamic magnetic properties, as could be shown by the temperature dependence of the D values. The most striking structural difference between the two orientations is the intermolecular distance to a nonbonded solvent (Et_2O) molecule. Results from DFT calculations on truncated model compounds (lacking the M_2 unit) support the influence of the Et_2O molecule on the D value of the Mn(II) ions, but do not suggest this interaction as the major contribution. Similarly, DFT calculations of ΔE_Q at various Fe−Cl distances in the truncated model **1m** show much a smaller sensitivity to the structural changes as observed experimentally. It is therefore proposed here that the quadruply bonded M≡M unit magnifies the magnetic anisotropy of Fe in **1** and Mn in **3** to an unprecedented extent that allows spectroscopic differentiation of two nearly identical metal sites. This physical phenomenon has, to our knowledge, not been observed before, and it creates a challenging new problem for theory, and opens up the possibilities of site-specific magnetic excitations, or transferring a microwave quantum between two sites where their EPR signals overlap.

Acknowledgment. We thank the National Science Foundation for support under CHE-0745500 and CHE-0741901 (Bruker ElexSys EPR).

Supporting Information Available: Crystallographic files, additional figures and a table of crystallographic data. This material is available free of charge via the Internet at http://pubs.acs.org.

JA106510G

(30) Hill, S.; Edwards, R. S.; Jones, S. I.; Dalal, N. S.; North, J. M. *Phys. Rev. Lett.* **2003**, *90*, 217204–217207.